



# Performance evaluation of tropospheric correction model for GBAS in China

Yanbo Zhu<sup>1</sup> · Honglin Tang<sup>1</sup> · Zhipeng Wang<sup>1</sup> · Kai Guo<sup>2</sup> · Shujing Wang<sup>1</sup> · Yiming Wang<sup>1</sup>

Received: 9 August 2023 / Accepted: 24 March 2024 / Published online: 23 April 2024  
© The Author(s), under exclusive licence to Springer-Verlag GmbH Germany, part of Springer Nature 2024

## Abstract

Ground-based augmentation system (GBAS) is a safety of life system that supports precision approach, landing, departure and surface operations in civil aviation. To compensate the tropospheric delay difference encountered at the aircraft and ground stations, empirical tropospheric correction (TC) models are applied. Scale height is one of the key parameters in TC models, while there are various methods to estimate scale heights and their performance is not fully evaluated, which affects the integrity and poses threats to GBAS. The purpose of this study is to evaluate the performance of TC models when using different scale height estimation methods by exploiting analytical products, including the European center for medium-range weather forecasts and meteorological data from the stations deployed in the crustal movement observation network of China in 2021. Taking the effects of virtual temperature and station height anomaly into consideration, a modified ray-tracing algorithm is proposed to calculate the tropospheric delay error, which is the difference of tropospheric delay between that encountered, respectively, at the GBAS station and the aircraft. The calculated tropospheric delay error serves as a reference to evaluate the performance of TC models. Results show that the TC model bias in the zenith direction estimated by the different scale height methods is approximately equal in the GBAS approach service type C. When the elevation is lower than 20°, there is a significant bias induced by the mapping function of TC models. Additionally, the TC model bias increases with height for GBAS precision approach service. The maximum TC model bias in the zenith direction at most stations exceeds 20 mm. The occurrence probability of anomaly with TC model bias more than 10 mm with a higher than 20% at a height of 400 m. This study contributes to better understanding of the GBAS TC model performance in China. It provides valuable insights and guidance for developing more precise TC models.

**Keywords** GBAS · Tropospheric correction model · Tropospheric delay error · Ray tracing · Mapping function

## Introduction

To ensure the precision and integrity of precision approach and landing under category (CAT)-I/II/III requirements in civil aviation, ground-based augmentation system (GBAS) employs differential techniques and anomaly monitoring algorithms to ensure user safety (Saito et al. 2017). The tropospheric delay emerges as a prominent source of error, particularly during tropospheric anomalies (Khanafseh et al. 2016). Based on the single differential positioning

method, it is commonly assumed that the zenith total delay (ZTD) is approximately equal between the ground reference stations and the user aircraft. However, due to the fact that the ground reference stations and aircraft are situated at different heights, difference exists in the tropospheric delay encountered, respectively, at the ground stations and the aircraft. This difference, defined as the tropospheric delay error in this studied, is corrected using the tropospheric correction (TC) models in differential corrections (RTCA 2004). It should be noted that if it is not specified that the tropospheric delay error refers to difference in the tropospheric delay encountered at the aircraft and ground stations.

The application of TC model in aeronautical navigation, especially in GBAS, was shown to improve positioning accuracy and reduce integrity risk (Skidmore and van Graas 2004; McGraw 2012). However, the calculation formulas for the

✉ Kai Guo  
guokai@buaa.edu.cn

<sup>1</sup> School of Electronics and Information Engineering, Beihang University, Beijing 100191, China

<sup>2</sup> Institute of Artificial Intelligence, Beihang University, Beijing 100191, China

scale height parameters used in TC models are not fully confirmed in GBAS. There are four different scale height calculation methods, i.e., McGraw et al. (2000), Skidmore and van Graas (2004), Warburton (2010) and Saito et al. (2021). It should be noted that the tropospheric delay error is relatively minor. However, clarification is important because it can also cause potential safety issue and should be carefully considered in future applications that require high accuracy (Saito et al. 2021). Furthermore, the performance of the four different scale height calculation methods used in TC models is not comprehensively evaluated in literature, which poses threats to the application of GBAS with different scale height methods and may cause performance degradation. Therefore, it is essential to assess the performance of the TC models with different scale height estimations and verify their compliance with the relevant GBAS standards. This contributes to developing a more accurate model, which further helps to mitigate tropospheric delay errors, ensure aircraft safety in extreme conditions and separate it with other parameters such as location and receiver clocks (Wang et al. 2022).

To evaluate the performance of the TC models, an approach is the ray-tracing techniques based on numerical weather models (NWMs) (Hobiger et al. 2008; Nafisi et al. 2012). The basic principle of ray tracing is geometrical optics approximation. The Eikonal equation is the key result of this approximation, which is used to describe electromagnetic waves passing through slowly varying media (Born and Wolf 1999). The equation is solved by partial derivative equations based on analytical method. However, the ray-tracing algorithm based on this equation takes more time due to the iteration process (Hobiger et al. 2008). Under the assumption that the refractive index profile is composed of almost constant gradients, Thayer (1967) modeled the refractivity index as radial distance power-law profile function. Results indicated its obvious advantages in accuracy, calculation speed and compatibility with previous results. Additionally, Hobiger et al. (2008) proposed a refined piecewise linear propagation algorithm by using Snell's law. The average refractivity index above and below half-height between two layers was calculated. Since the ray path can be calculated in a single calculation, the computational cost is significantly reduced. Ray-tracing algorithm based on piece-wise linear method was applied to very long baseline interferometry (VLBI) and interferometric synthetic aperture radar (InSAR) analysis (Hofmeister and Böhm 2017). Hobiger et al. (2010) studied the calculation biases caused by the rapid change of wet refractivity due to the use of simplified ray-tracing algorithm in InSAR data processing. Tropospheric tomography based on ray-tracing algorithm is also widely used to estimate three-dimensional distribution of water vapor (Haji Aghajany and Amerian 2017; Zhang et al. 2022). However, the above algorithms mostly pay attention to the calculation accuracy and speed, there is

little research on the requirements of data input to model the whole meteorological information between the ground and the aircraft. For example, it is difficult to capture the meteorological information of the lower atmosphere using only NWM products for ray tracing. For GBAS approach service type C (GAST-C), the decision height is less than 200 ft. Therefore, the decision height may be lower than the height of the lowest ERA5 product, which is approximately 492 ft. In this case, the conventional ray tracing is not applicable.

To address the issues above, this study proposed a modified ray-tracing algorithm that utilizes both the station surface and the upper-air meteorological data to calculate the tropospheric delay error. The effect of virtual temperature and station height anomaly are also considered to improve the accuracy of tropospheric delay error estimation and unify the spatial datum of different data. The estimated tropospheric delay error is then used to assess the performance of the TC models based on four scale height estimation methods. The principle of GBAS TC model is reviewed next. The modified ray-tracing algorithm is then present, followed by the description of the datasets. The performance of the TC models using four different scale height estimation methods is evaluated. Finally, conclusions and remarks are presented.

## Overview of the TC models for GBAS

This section introduces the description of TC models in GBAS. The four different scale height calculation methods for the TC models are also reviewed.

### GBAS TC models

To correct the tropospheric delay error, which is the difference of tropospheric delay between that encountered, respectively, at the GBAS ground station and the aircraft, as shown by a simplified differential architecture in Fig. 1, the TC model is applied in differential corrections. The model and its uncertainty are defined as (RTCA 2004, 2017)

$$TC = N_R h_0 \frac{10^{-6}}{\sqrt{0.002 + \sin^2(\theta)}} \left( 1 - \exp\left(-\frac{\Delta h}{h_0}\right) \right) \quad (1)$$

$$\sigma_{\text{trop}} = \sigma_N h_0 \frac{10^{-6}}{\sqrt{0.002 + \sin^2(\theta)}} \left( 1 - \exp\left(-\frac{\Delta h}{h_0}\right) \right) \quad (2)$$

where  $1/\sqrt{0.002 + \sin^2(\theta)}$  is the mapping function (MF) related to the satellite elevation  $\theta$ .  $N_R$  is the surface refractivity index.  $\sigma_N$  is the uncertainty in the refractivity index.  $h_0$  is the tropospheric scale height.  $\Delta h$  is height of the aircraft relative to the GBAS station.

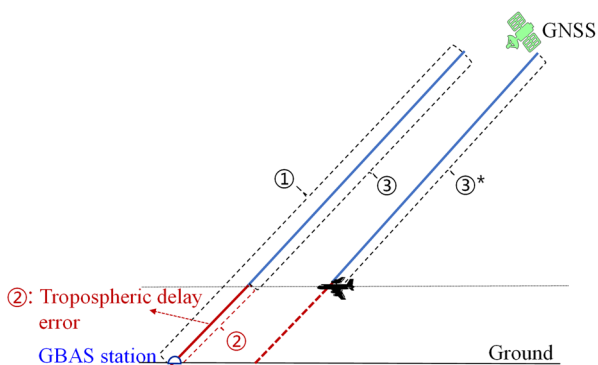


**Fig. 1** A simplified GBAS differential architecture. The tropospheric delay error is the difference of tropospheric delay between that encountered, respectively, at the GBAS station (path ①) and the aircraft (path ③\*). The tropospheric delays of path ③ and path ③\* are approximately equal in short-baseline differential positioning. The tropospheric delay error is corrected by the tropospheric correction model in GBAS

The TC model in the zenith direction, denoted as  $TC_{zd}$ , is the integral of refractivity index profile (Saito et al. 2021), i.e.,  $TC_{zd} = 10^{-6} \int N_R \exp\left(-\frac{\Delta h}{h_0}\right) dh = 10^{-6} N_R h_0 \left(1 - \exp\left(-\frac{\Delta h}{h_0}\right)\right)$ . The formula employs the exponential function and scale height to characterize the vertical variation of refractivity index. The uncertainty of the TC model is determined through the variance–covariance propagation law. It should be noted that the variation of scale height is disregarded and assumed to be constant in Equation (2).

### Scale height estimation methods in TC models

Estimating the TC model parameters is essential for accurately compensating the tropospheric delay error. Using the four different methods, the scale height can be estimated as constant annual averaged values or real-time variations, while under extreme weathers during system operation, it is not reasonable to treat the scale height as a constant value. Although real-time estimation can potentially yield better performance, there are countries currently utilizing an annual averaging scheme. In this analysis, the scale height is used as a constant to evaluate the performance of the TC model under the worst conditions. For the sake of illustration, the scale height estimation follows the methods provided in McGraw et al. (2000), Skidmore and van Graas (2004), Warburton (2010) and Saito et al. (2021), which are referred to as method 1, 2, 3 and 4, respectively, in this study.

Figure 2 shows the variations of the tropospheric delay error estimated by the TC models using four scale height estimation methods at a height of 6 km at various elevations. It is evident that the tropospheric delay error calculated with different methods exhibits more similarities

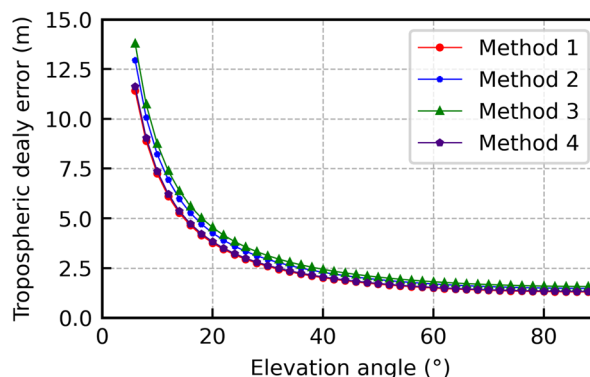


**Fig. 2** Variations of tropospheric delay error calculated among different scale height methods at various elevations. The cutoff elevation is  $6^\circ$

at higher elevations, while as the elevation decreases, the deviations between different methods present more disparities, which are due to the error induced by the MF. When the elevation angle is  $6^\circ$ , the disparities between different models reach their maximum.

Figure 3 presents the calculated scale heights by four different methods at the BJSH in Beijing, China, using meteorological data from the crustal movement observation network of China (CMONOC) in 2021. The average bias between the scale heights calculated by different methods is 9.2 km, and the maximum bias is 12.6 km. Additionally, the calculated scale heights with method 2 show a completely opposite seasonal variation in contrast to the other methods. Due to the significant differences in scale heights calculated by the four different methods, it is necessary to further evaluate the performance of the TC models using four different scale height methods.

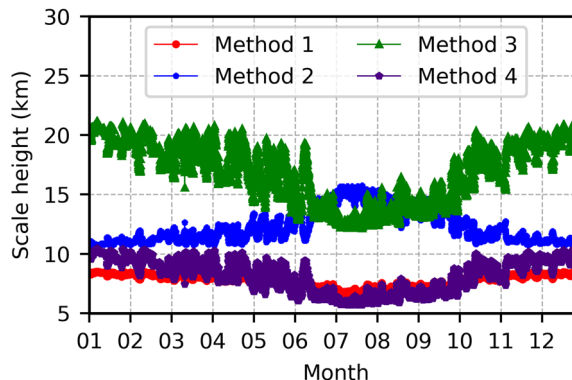


**Fig. 3** Scale heights calculated by four methods at the BJSH station in Beijing, China, in 2021

### Tropospheric delay error estimation by modified ray-tracing algorithm

As the relative and specific humidity contain different meteorological elements related to water vapor, these two humidity measurements are first converted to partial water vapor pressure based on empirical models. Additionally, to reduce the influence of layer height on the integration errors and efficiency of ray-tracing algorithm, the optimal layer height is determined next. With the convert partial water vapor pressure and determined optimal layer height, the modified ray-tracing algorithm is established to estimate the tropospheric delay error.

#### Partial water vapor pressure conversion

The well-known expression for the refractivity index of the troposphere is given by (Thayer 1974)

$$N = k_1 \frac{p_d}{T} Z_d^{-1} + k_2 \frac{e}{T} Z_w^{-1} + k_3 \frac{e}{T^2} Z_w^{-1} \tag{3}$$

where  $T$  is the temperature in Kelvin.  $p_d$  and  $e$  are the dry and water vapor partial pressures in millibars, respectively.  $Z_d$  and  $Z_w$  are compression factors.  $k_1$ ,  $k_2$  and  $k_3$  are empiric constants, where  $k_1 = 77.604$  K/hPa,  $k_2 = 64.79$  K/hPa and  $k_3 = 377600$  K<sup>2</sup>/hPa.

Since the ground and upper atmosphere products utilize different meteorological parameters, the partial water vapor pressure can be calculated using the relative humidity at ground stations (McCarthy and Petit 2004; Leandro et al. 2006), i.e.,

$$e = \frac{RH}{100} e_{\text{sat}u} f_w \tag{4}$$

where RH is the relative humidity.  $e_{\text{sat}u}$  is the saturation vapor pressure.  $f_w$  is the enhancement factor given by

$$f_w = 1.00062 + 3.14 \times 10^{-6} P_0 + 5.6 \times 10^{-7} (T_0 - 273.15)^2 \tag{5}$$

The specific humidity of the upper atmosphere data of the fifth-generation European center for medium-range weather forecasts (ECMWF) re-analysis (ERA5) is converted to partial vapor pressure, which is given by (Wallace and Hobbs 2006; Nafisi et al. 2012)

$$p_w = \frac{qp}{(\epsilon + (1-\epsilon)q)} \approx \frac{qp}{(0.622 + 0.378q)} \tag{6}$$

where  $p$  denotes the total pressure.  $q$  is the specific humidity.  $\epsilon = M_w/M_d$  is the ratio of the molar masses of water vapor and dry gas.

### Determining the optimal layer height

By ray tracing the neutral atmosphere NWMs along the path @ in Fig. 1, the tropospheric delay error, referred to as  $D_{\text{trop}}$ , can be estimated by

$$D_{\text{trop}} = 10^{-6} \int N ds = 10^{-6} \sum_{i=1}^k N_i s_i \tag{7}$$

where  $k$  is the number of height layers (Zhou et al. 2020).  $N_i$  is the refractivity of the  $i$ th layer.

To minimize numerical integration errors and ensure calculation efficiency, a trade-off is made between the layer height and the computational error. Figure 4 shows the relationship between the layer height and the integration errors at different elevations. As the layer height decreases, the integration error also decreases. However, the time consumption also increases, which is shown as the purple line in the figure. It should be noted that the calculation of the time consumption is based on a laptop with 16 G random access memory (RAM) and Intel i5-10300H@2.50 GHz processor, thus the calculation time may differ at different platforms. The figure indicates that the integration errors converged when the layer height is less than 1 m. Further reducing the layer height only slightly improves the integration accuracy, while significantly increasing computation time, which largely limits the algorithm performance. Therefore, to achieve a balance between computation time and integration errors, an integration layer height of 1 m is chosen for this study.

#### Modified ray-tracing algorithm establishment

In order to unify the spatial datum of different products and improve the estimation accuracy of tropospheric delay error, a modified ray-tracing algorithm is proposed that considers

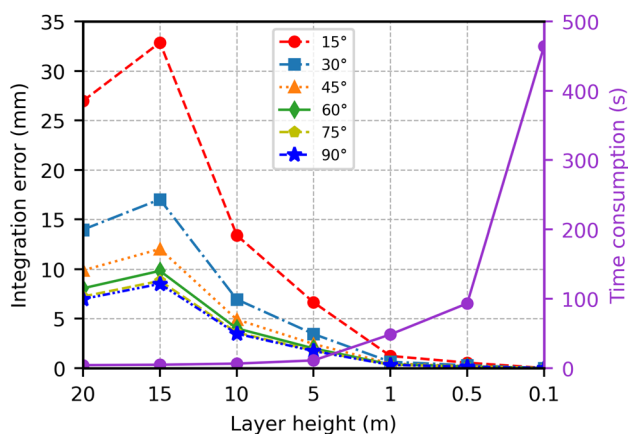


Fig. 4 Variations of integration errors and time consumption at different elevations when using different integration layer heights

height anomaly and virtual temperature. The decision height of an aircraft is typically less than 60 m in CAT I, while the height anomaly based on EGM96 may exceed 80 m in China. Therefore, this induces a discrepancy between the height of calculated tropospheric delay error and the actual height. On the other hand, by introducing virtual temperature, we can express the presence of moisture in the air using the dry air equation of state. In the calculation of the overall ZTD, the virtual temperature correction is generally negligible compared with the model error. However, according to equation (10) for the virtual temperature hereafter, the correction for virtual temperature cannot be neglected, as it is directly proportional to the temperature and water vapor content (Sheng et al. 2013). Therefore, the effect of virtual temperature and height anomaly are considered in the modified ray-tracing algorithm. Moreover, the modified algorithm not only utilizes ERA5 products but also incorporates meteorological data from ground stations. Since the integration height is very low, the Fresnel effect can be disregarded. Additionally, the vertical resolution of the ERA5 data is improved using a meteorological parameter profile, which is described in details in the subsequent sections.

The proposed algorithm consists of three main steps, i.e., (1) Calculating the longitude and latitude of the tropospheric piercing point (TPP) and the horizontal meteorological parameters using the bilinear interpolation algorithm. (2) Determining the vertical meteorological parameters at any given altitudes, which allows for the calculation of meteorological elements at various layers between the ground station and the aircraft. (3) Computing the tropospheric delay error along the signal propagation path using a hierarchical integration algorithm based on the refractivity index profile. Figure 5 presents the flowchart of the modified ray-tracing strategy.

The establishment of atmospheric pressure, temperature and water vapor pressure profiles are the key aspect in estimating the tropospheric delay error. The temperature profile is influenced by the thermal characteristics of the atmosphere and the thermal balance of the Earth. In the tropospheric region below 10 km, the temperature profile exhibits a linear decrease given by (Chao 1974).

$$T = T_s - \alpha(h - h_s) \tag{8}$$

where the subscript  $s$  refers to the GBAS station.  $h$  is the height of the aircraft in kilometers.  $\alpha$  is the temperature lapse rate. It is worth mentioning that since the distance between neighboring pressure layers at the bottom of the ERA5 product is only a few hundred meters, the linear temperature lapse rate, which is only used to describe the temperature change between the neighboring pressure layers of ERA5 products, can accurately capture real atmospheric changes (Hobiger et al. 2008; Zhou et al. 2020).

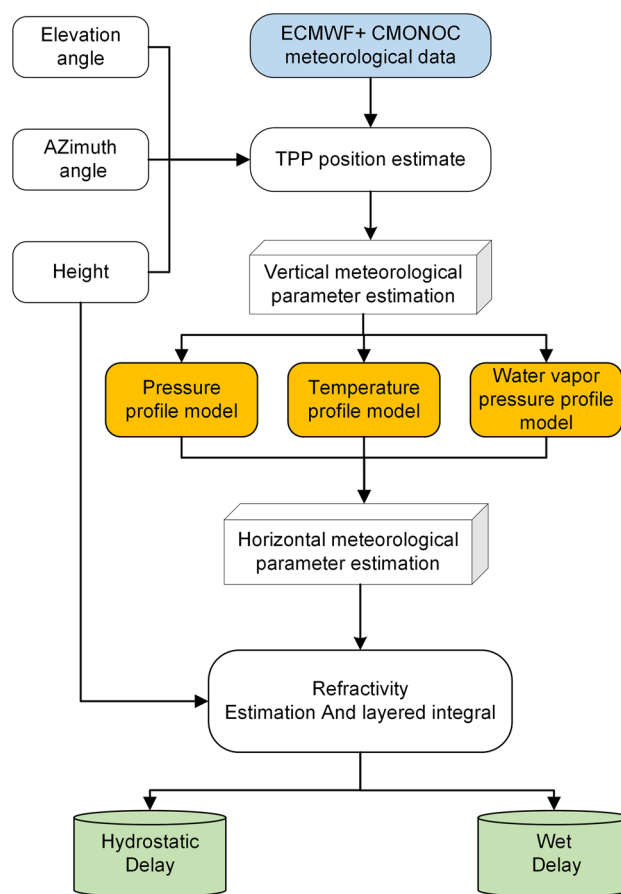


Fig. 5 Flowchart of modified ray-tracing strategy

According to the multivariate atmospheric hypothesis, the pressure profile is defined as (Hopfield 1971; Davis et al. 1985)

$$P = P_s \left[ 1 - \frac{\alpha(h-h_s)}{T_v} \right]^{\frac{g}{R_d \alpha}} \tag{9}$$

where  $g$  is the gravitational acceleration.  $R_d$  is the gas constant.  $T_v$  is the virtual temperature instead of the actual temperature, which is defined as (Sheng et al. 2013)

$$T_v = (1 + 0.608q)T = (1 + 0.378e/p)T \tag{10}$$

It is evident that higher temperature contributes to the increase in water vapor pressure and subsequently larger corrections for virtual temperature. Therefore, the effect of virtual temperature cannot be ignored. On the other hand, the vertical variation of water vapor pressure profile can be approximated to exponential attenuation, which is defined as (Askne and Nordius 1987)

$$\frac{e}{e_s} = \left( \frac{P}{P_s} \right)^{\lambda+1} \tag{11}$$



where  $\lambda$  is the water vapor pressure height factor.  $e_s$  and  $P_s$  are the water vapor pressure and pressure at the GBAS station, respectively.

It is worth mentioning that although the modified ray-tracing algorithm creates temperature and pressure profile between the two layers of products, it essentially uses the numerical summation method. Thus, the computational performance of the algorithm is approximately equal at different elevations, where the computational performance is indicated by the average time required to calculate the tropospheric delay error for a given elevation and azimuth at a particular epoch (Hobiger et al. 2008). For precision approach, CAT-I and CAT-III phases, it, respectively, takes 385, 245 and 236 ms for using the modified ray-tracing algorithm. Except for the time-consuming for CMONOC, ECMWF products and other data input and output, the interpolation is another key factor that limits the algorithm performance.

## Datasets

To estimate the tropospheric delay error, an accurate characterization of both the surface conditions at the station and the upper-air meteorological environment is crucial. The surface meteorological data is obtained by Paroscientific model 760 meteorological sensors deployed in CMONOC, which are widely applied in various fields, including geodesy and weather forecasting (Shi et al. 2018). Additionally, to cover typical climatic environment at different latitudes in China, 13 ground meteorological stations are selected which are located in various regions, as depicted in Fig. 6.

The time span is from January to December 2021. The sampling interval is 30 s. It should be clarified that according to the international civil aviation organization-navigation

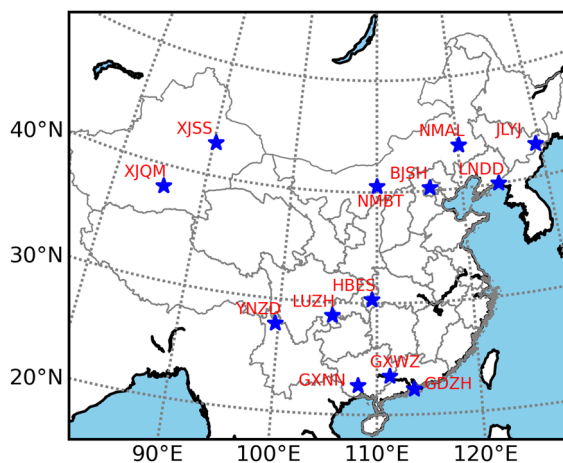


**Fig. 6** Geographic distribution of the selected CMONOC meteorological stations

systems panel (ICAO-NSP), the duration of data required for estimating TC model parameters is at least one year (Saito et al. 2022). Consequently, the length of the dataset used in this study meets the requirements. On the other hand, it is obvious that there are significant differences in tropospheric conditions in different regions, thus the dataset is not globally representative and can only be used to evaluate the performance of the TC models in China.

Reanalysis products, including the ERA5, play a crucial role in estimating and modeling tropospheric delays. ERA5 is particularly notable for its exceptional performance, thanks to its high temporal and spatial resolution (Zhou et al. 2020). In this study, the upper atmosphere data derived from ERA5 is also processed. The data has a horizontal resolution of  $0.25^\circ \times 0.25^\circ$  in latitude and longitude, as well as a vertical resolution of 37 pressure levels. The sampling interval is 1 h. It should be noted that the ERA5 data refers to the geoid over land in the vertical direction, i.e., Earth gravitational model 1996 (EGM96). However, the spatial datum of CMONOC data is world geodetic system 1984 (WGS84). Therefore, to ensure the unification in the spatial datum, the EGM96 model is utilized to calculate the height anomaly of the ground station. Table 1 lists the selected ground stations, height anomaly and the corresponding climatic types (Song et al. 2011).

## TC model performance evaluation

By utilizing the modified ray-tracing algorithm, reference values for tropospheric delay error in the zenith and slant direction are calculated to evaluate the performance of TC models with the four scale height estimation methods. Moreover, an inflation algorithm based on elevations is introduced to overbound the bias associated with the TC model.

### TC model evaluation in the zenith direction

The performance of TC models with different scale height estimation methods is evaluated by calculating the tropospheric delay error in the zenith direction using meteorological data from 2021. The TC model bias, defined as the deviations with the reference tropospheric delay errors estimated by the modified ray-tracing algorithm, is calculated and analyzed.

Figure 7 depicts the TC model bias for four representative CMONOC stations with four different scale height methods in January 2021. Simulations are conducted for CAT I mode. The selected four stations represent diverse climate environments, encompassing various longitudes and latitudes. Despite employing different scale height estimation methods, the TC model bias for the same site is almost identical, primarily due to the low decision height. The TC model bias

**Table 1** Locations, height anomaly and the climate types of the selected meteorological stations

Station	Latitude (°N)	Longitude (°E)	Ellipsoidal height (m)	Height anomaly (m)	Climatic type
YNZD	27.82	99.70	3297.07	−33.09	Subtropical monsoon
LUZH	28.87	105.41	298.25	−40.09	Subtropical monsoon
HBES	30.28	109.49	473.36	−24.67	Subtropical monsoon
NMBT	40.60	110.02	1054.03	−28.08	Temperate continental
XJQM	38.12	85.53	1203.06	−56.10	Temperate continental
XJSS	42.89	90.26	348.77	−63.86	Temperate continental
BJSH	40.25	116.22	87	−9.01	Temperate monsoon
JLYJ	42.87	129.5	284.71	26.07	Temperate monsoon
NMAL	43.86	120.11	377.83	1.04	Temperate monsoon
LNDD	40.03	124.33	31.93	15.49	Temperate monsoon
GDZH	22.28	113.57	51.49	−3.86	Tropical monsoon
GXWZ	23.48	111.23	63.78	−14.73	Tropical monsoon
GXNN	22.57	108.15	97.91	−23.87	Tropical monsoon

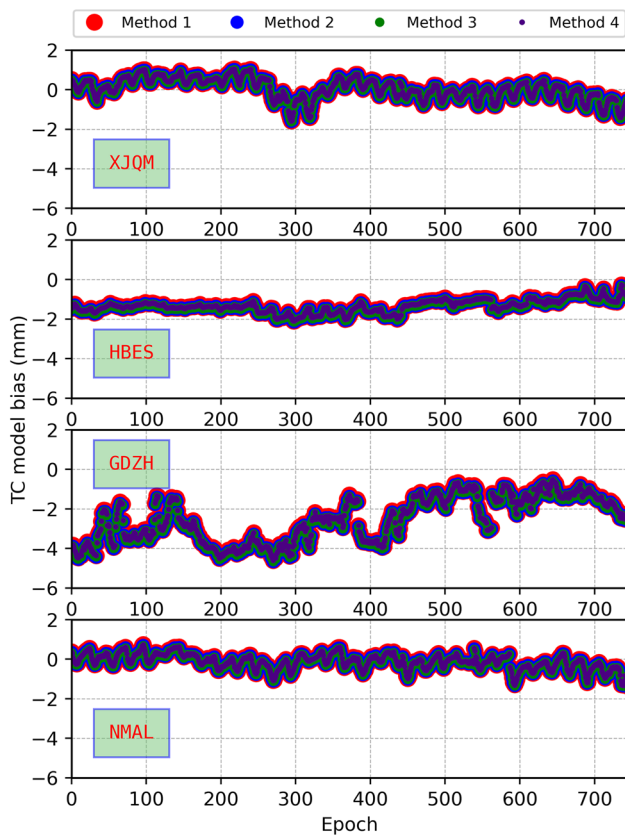


**Fig. 7** Variations of TC model bias at XJQM, HBES, GDZH and NMAL stations in January 2021

is mainly affected by the airport surface meteorological elements. As a result, the similar results obtained by different scale height methods are due to the lack of rapid changes in meteorological elements. At the same time, this also answers which scale height estimation method should be used to

estimate the tropospheric delay error in China. Furthermore, the figure illustrates distinct bias trends at the four stations, which are primarily influenced by local climate conditions.

To further analyze the influence of local climate on the TC model performance, Fig. 8 shows the relationship between ground water vapor pressure and refractivity index at a height of 60 m in 2021. The top two panels show the changes of ground water vapor pressure at YNZD and GDZH stations, while the middle two panels show refractivity index changes calculated by interpolating ERA5 and CMONOC product, empirical refractivity index model, i.e.,  $N_{60\text{ m}} = N_R \exp(-60/h_0)$  at a height of 60 m. The parameters of the empirical refractivity index model are calculated by annual average and real-time methods, respectively. Results show that the TC model using the annually average method is unable to capture the local climate variation, as shown in the middle panel. On the contrary, compared with EAR5, the real-time estimation shows excellent performance. Therefore, the real-time refractivity index and scale height estimation should be used in precision approach to mitigate the effect of climate variation. In addition, the bottom two panels show that there is a high correlation between ground water vapor pressure and refractivity index bias, which implies that the bias of the refractivity index is influenced by the ground water vapor pressure.

Figure 9 illustrates the distribution of the TC model bias in the zenith direction across 13 ground stations operating in GAST-C. It can be seen that the average bias remains consistency among different regions, with the mean values fluctuating around 0. However, the bias distribution at each station is obviously deviated with Gaussian distribution, which is commonly used to describe TC model bias. This bias is probably due to the fact that the scale height variations related to seasons are not considered. The tropospheric anomaly is considered to be the extreme

**Fig. 8** Surface water vapor pressure and refractivity index at a height of 60 m at YNZD and GDZH stations. The panels from the top to bottom represent the variation of surface water vapor pressure, the refractivity index estimated by interpolating ERA5 and CMONOC product, empirical refractivity index model and variations of the refractivity index bias as a function of ground water vapor pressure

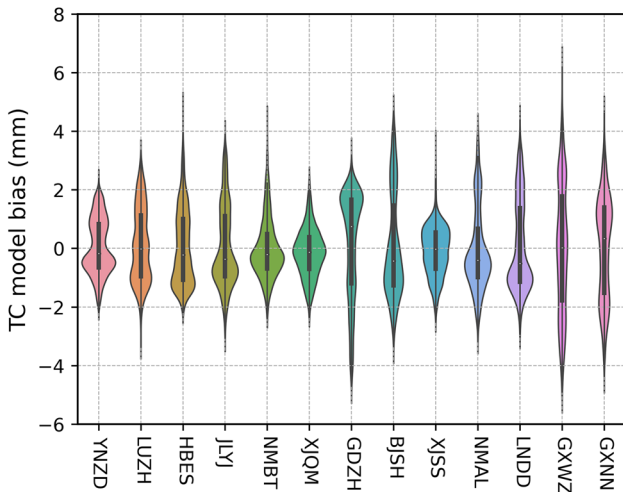
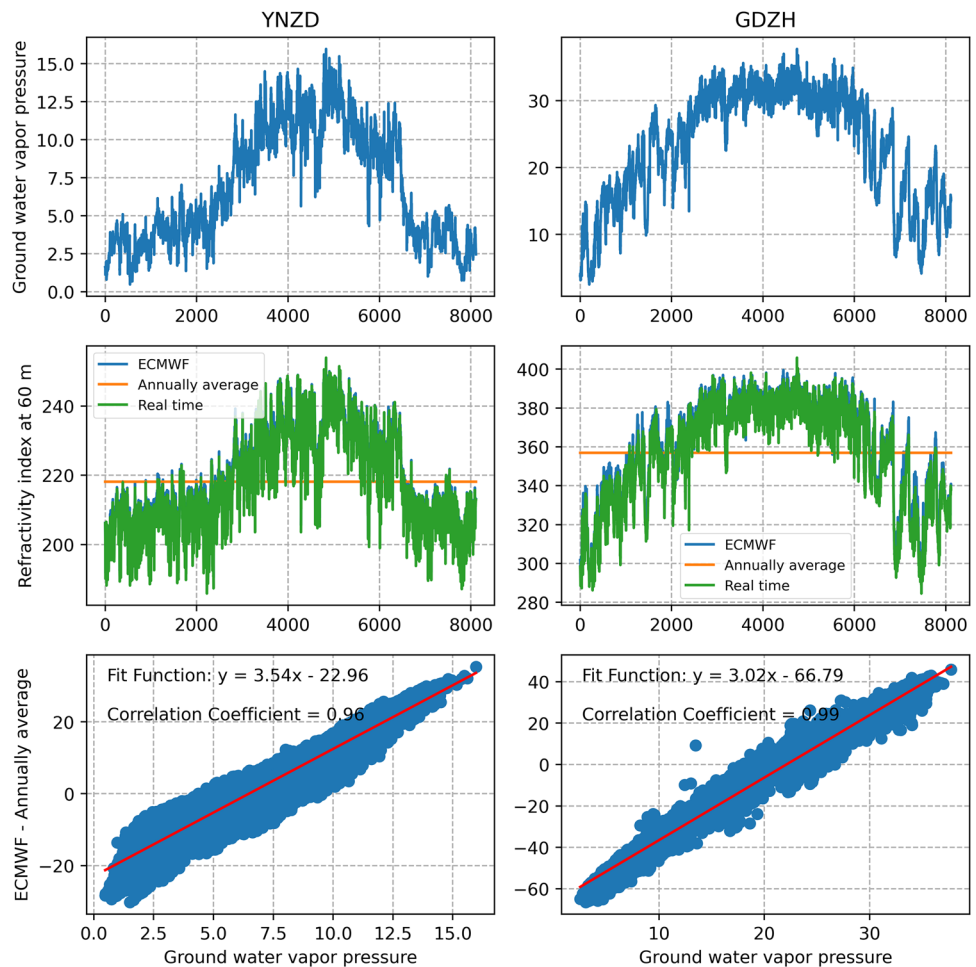


**Fig. 9** The distribution of the TC model bias in the zenith direction estimated at the 13 ground stations in GAST-C

point at both ends of the violin curves. A higher probability of the tropospheric anomaly is occurrence observed in low latitude regions. Compensating for the tropospheric

delay error using empirical TC model becomes challenging during extreme weather events such as inversion layers. Therefore, it is crucial to consider monitoring extreme weather-related tropospheric phenomena to ensure system safety for GBAS in the future. It is important to note that GDZH, GXWZ and GXNN stations exhibit more extreme TC model bias compared with others. This can be attributed that all three stations are situated at low latitudes, making them more susceptible to subtropical monsoon climates with more frequent extreme weather events.

Figure 10 presents the TC model bias based on Method 1 at different altitudes at BJSH station. It can be seen that the model bias gradually increases with height. Similar results are observed for other scale height estimation methods, although not shown here. This behavior can be attributed to the employed modeling framework of the TC model, which utilizes a whole modeling approach with an exponential function and scale height to describe the variation of the refractivity index profile. However, with the height increases, the complexity of variations intensifies in meteorological elements, leading to more challenges for



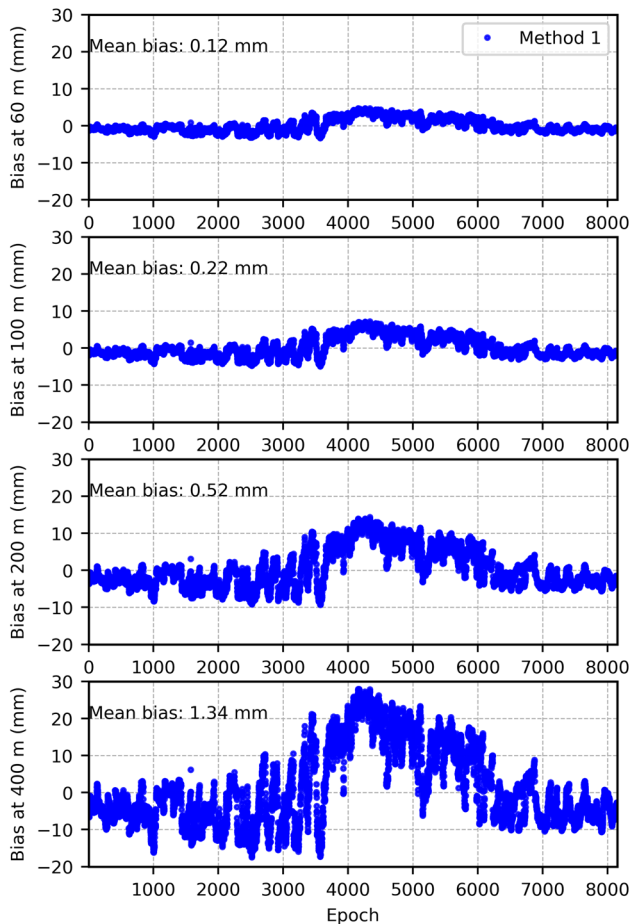


**Fig. 10** Variations of the TC model bias at altitudes of 60, 100, 200 and 400 m based on the scale height estimation method described in McGraw et al. (2000) at BJSH station in 2021

the scale height to accurately capture the actual variations in refractivity index.

Table 2 summarizes the accuracy of the TC model in the zenith direction at different heights corresponding to the results shown in Fig. 10. At a decision height of 60 m, the TC model achieves an average bias of 0.12 mm and an RMS of 1.76 mm, meeting the precision landing requirements for CAT I. However, the average bias increases to 1.34 mm, and the RMS reaches 10.38 mm at a decision height of 400 m. Although the average bias is very small, the presence of large TC model biases, which exceed the range assured by

**Table 2** Statistics of the TC model bias and RMS at heights of 60, 100, 200 and 400 m based on the scale height estimation method described in McGraw et al. (2000) at BJSH station in 2021

Altitudes (m)	60	100	200	400
Bias (mm)	0.12	0.21	0.52	1.34
RMS (mm)	1.76	2.67	5.28	10.38

the broadcasted uncertainty of the TC model, can cause loss of integrity. Additionally, the increased RMS value leads to a larger protection level, subsequently reducing system availability. On the other hand, a comprehensive tropospheric threat model, encompassing all potential tropospheric anomaly conditions, is essential for ensuring aircraft safe (Khanafseh et al. 2016). With the increase in height, the TC model bias is no longer influenced by the surface meteorological elements, the tropospheric refractivity index profile based on the exponential function is difficult to capture the change of refractivity index with height. Consequently, the TC model bias gradually increases with height.

**TC model evaluation in the slant direction**

With the assistance of the proposed ray-tracing algorithm, it becomes possible to evaluate the TC model bias associated with the MF in the slant direction. This section evaluates the performance of MF at different stations and seasons. Figure 11 presents the TC model bias in the slant direction at different elevations and azimuths in GAST-C on January 1, 2021. It can be seen that the TC model bias at different stations is smaller at higher elevations. Meanwhile, the anisotropy of the TC model bias across different azimuths is not pronounced. However, with the elevation decreases,

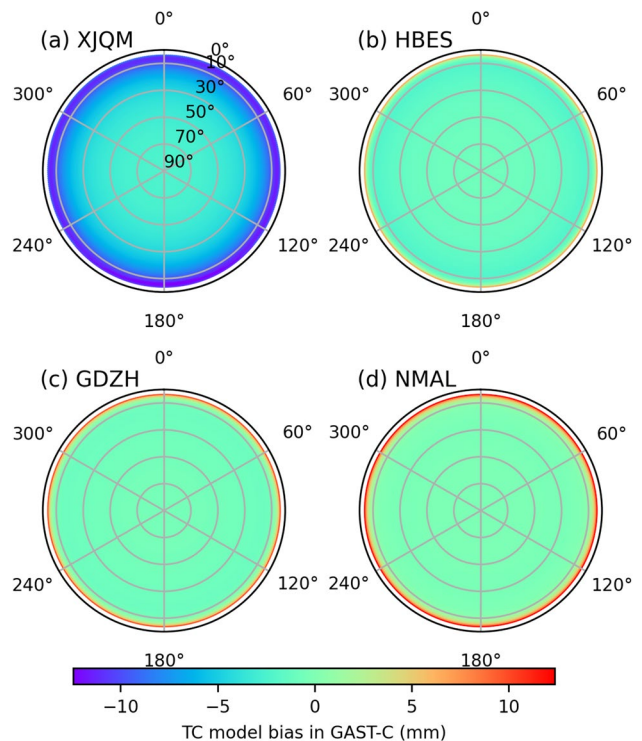


**Fig. 11** The TC model bias at XJQM, HBES, GDZH and NMAL stations at different elevations and azimuths in GAST-C. The cutoff elevation angle is 6°

the model bias increases with the decrease in elevations. The TC model bias reaches its maximum at an elevation of 6°. It should be noted that GBAS provides aircraft with differential corrections and integrity information for satellites with an elevation greater than 5° using very high frequency (VHF) data broadcasting stations (Saito et al. 2017). Therefore, considering the fact that the GBAS standard sets the cutoff elevation at 5°, this discrepancy leads to a larger TC model bias. The primary reason of the bias lies in the MF, which exhibits noticeable systematic bias at low elevations. To mitigate the impact of the MF-induced TC model bias on integrity, the systematic bias needs to be overbounded. Moreover, a more precise MF can also be developed to mitigate the effect of MF errors on GBAS.

To investigate the performance of the TC model in different seasons, the scale height estimation method described in McGraw et al. (2000) method is utilized and the TC model bias is calculated at the BJSH station, as presented in Fig. 12. It is observed that the bias is larger at low elevations. Additionally, the bias is significantly larger in summer compared with other seasons. This is caused by a couple of reasons. Firstly, the abundance of water vapor in summer induces challenges in accurately estimating the refractivity index due to pronounced variations in wet delay. Secondly, it is difficult for the scale height using annual mean to

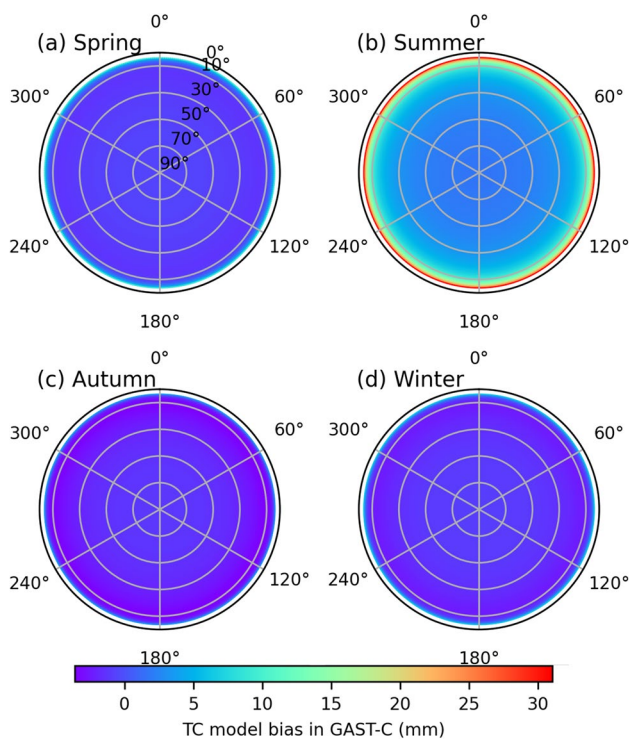


**Fig. 12** The TC model bias at different elevations and azimuths in different seasons in GAST-C. The cutoff elevation angle is 6°

accurately describe the tropospheric delay error at stations experiencing significant seasonal changes.

To further analyze the effect of seasonal variation on the TC model performance,

the TC model bias in different seasons in GAST-C at the BJSH station is shown in the top panel in Fig. 13. It can be seen that seasonal variations are obvious. The wet component in the tropospheric delay error derived by the modified ray tracing is also shown in the second panel. A similar trend can be found between the TC model bias and the wet component, which is further verified by the correlation analysis in the third panel, indicating that the variation of the TC model bias is mainly influenced by the wet delay or water vapor in different seasons. To quantitatively evaluate the impact of seasonal changes on the TC model, the bottom panel shows that the tropospheric delay error is overestimated by the TC model during summer and autumn, reaching a maximum bias of 4.7 mm, while it is underestimated during spring and winter. The average bias of the TC model is in the millimeter magnitude. Therefore, similar to the conclusions from Fig. 8, the timely refractivity index and scale height

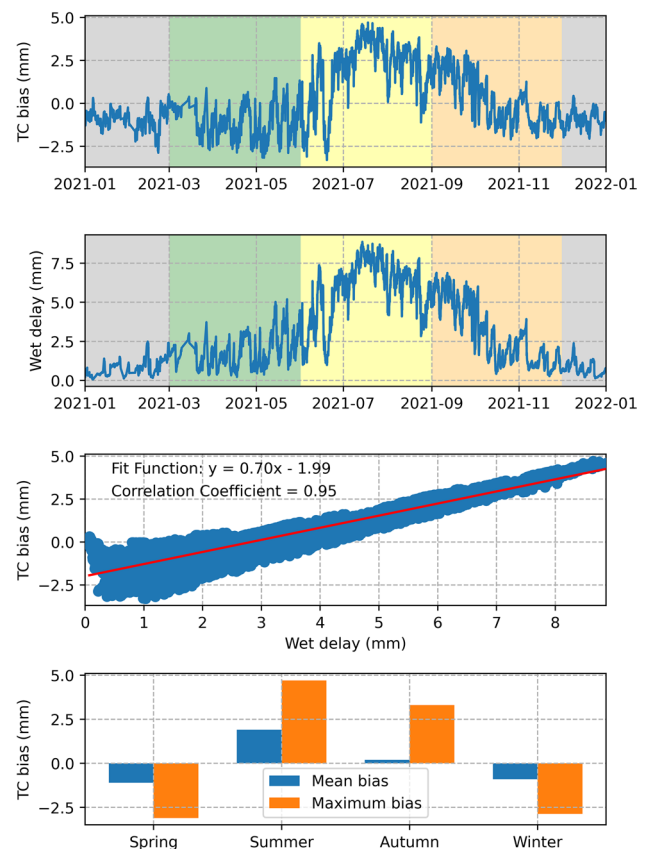


**Fig. 13** Variations of the TC model bias and wet component in GAST-C at BJSH station. The panels from top to bottom, respectively, represent the TC model bias, wet component in the tropospheric delay error, variation of TC model bias as a function of wet component and TC model bias statistics, respectively

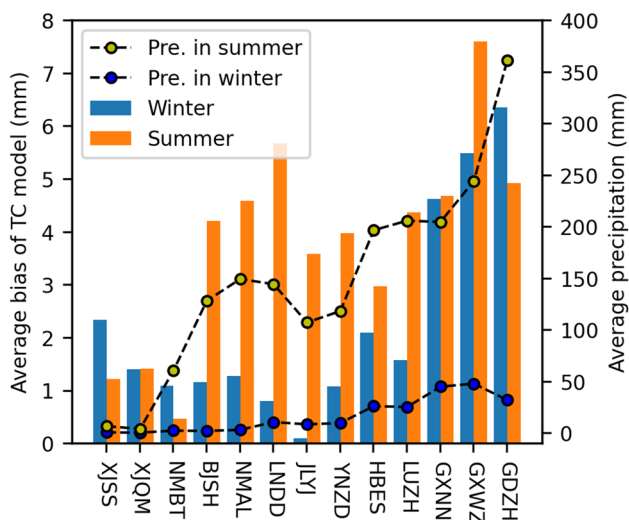


**Fig. 14** Comparison of the TC model bias and mean precipitation in summer and winter at 13 ground stations in 2021

estimation should be applied in precision approach to accurately capture seasonal variations and consequently estimating the tropospheric delay errors.

Figure 14 shows the seasonal bias of the TC model and the mean precipitation (Peng 2020) in summer and winter at 13 stations in 2021. It can be seen that the TC models at XJSS, XJQM and NMBT stations, characterized by a temperate continental climate, exhibit the highest accuracy. Furthermore, the seasonal changes in summer and winter are not significant at these stations with low precipitation. On the other hand, the bias of TC model shows obvious seasonal variation at BJSH, NMAL, LNDD and JLYJ stations in temperate monsoon climate. The performance of the models in winter, with an average bias of 0.83 mm, surpasses that in summer with a bias of 4.5 mm. The model bias also exhibits seasonal changes at YNZD, LUZH and HBES stations, which are characterized by a subtropical monsoon climate. However, in contrast to the previous four stations characterized by the temperate monsoon climate, the seasonal variations in the model’s average bias are reversed for summer and winter. The GXNN, GXWZ and GDZH stations with more precipitation demonstrate the poorest model performance, with an average bias of 5.6 mm in 2021. This is due to the fact that the scale height estimation method is more applicable to mid-latitudes. In other words, the surface temperature parameter in the scale height estimation is assumed to be 15 °C and is not applicable at low latitudes. Additionally, the figure highlights a relationship between the performance of the TC model and the average precipitation. The TC model, which is based on the scale height, models the refractivity index as a unified entity, without separating hydrostatic and wet component. Consequently, this modeling approach is less effective in estimating wet delay in theory.

This limitation leads to larger bias in regions with higher precipitation.

To further evaluate the performance of the TC model in extreme environments, the maximum TC model bias and occurrence probability of anomaly are calculated at various elevations at a height of 400 m, as shown in Fig. 15. The left two panels show the maximum TC model bias and occurrence probability of anomaly in the zenith direction. The threshold for anomaly determination in the zenith direction is set as 10 mm. It can be seen that the maximum bias at most of the stations exceeds 10 mm with an occurrence probability exceeding 20%. The maximum bias of 28 mm in the zenith direction is observed at BJSH station, as shown in the top left panel. Furthermore, compared with other stations, the panel in the bottom left shows that the probability of anomalies exceeds 41% at GDZH, GXNN and GXWZ stations, which are located at low latitudes. This can be attributed to the more complex variations in water vapor at low latitudes, leading to more frequent extreme weather events. On the other hand, the maximum TC model bias in the slant direction is shown in the top right panel. It can be seen that the maximum bias increases as the elevation decreases. The maximum TC model bias found at an elevation of 6° is 363 mm. To evaluate the occurrence probability of anomaly in the slant direction and mitigate the impact of the MF, the thresholds at different elevations are scaled up using the formula  $10/\sqrt{0.002 + \sin^2(\theta)}$ , as shown by the blue lines in the bottom right panel. The occurrence probability of anomaly remains stable at around 23% at higher elevations can be observed. However, there is a noticeable increase in

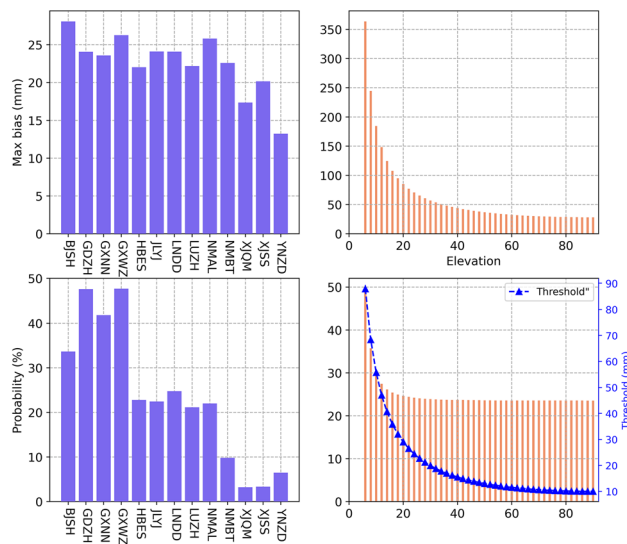


**Fig. 15** Statistics of the maximum TC model bias and occurrence probability of anomaly in the zenith and slant direction. The top two panels are the maximum TC model bias in the zenith and slant direction, respectively. The bottom two panels, respectively, represent the occurrence probability of anomaly in the zenith and slant direction

the occurrence probability of anomaly when the elevation is below 10°. This indicates that the MF performs poorly at low elevations, making it challenging for TC models to accurately estimate the actual tropospheric delay error.

### Uncertainty overbounding of TC model bias

Figure 16 depicts the TC model uncertainty and mean bias calculated for various elevations. The blue line represents the actual TC model uncertainty calculated using the modified ray-tracing algorithm, while the red line shows the theoretical uncertainty estimated based on equation (2) using the scale height method described in McGraw et al. (2000). Three representative stations, selected to represent airports situated at different latitudes with diverse climatic conditions, are included in the analysis. It can be observed that the actual and theoretical uncertainties exhibit a high level of consistency across almost all elevations.

It is commonly assumed that the TC model bias transmitted by the ground station should follow a zero-mean normal distribution. However, significant TC model bias between the actual and theoretical uncertainties is observed at low elevations in this analysis, as shown by the black lines in Fig. 16. These biases may lead to unacceptable integrity

risks. When the TC model bias deviates from a zero-mean Gaussian distribution, an overbounding method is required for airborne users. This renders the use of uncertainty overbounding to accommodate the presence of such the TC model bias. In theory, since the ground station possesses the knowledge of the parameters related to the error probability density function (PDF), overbounding nonzero-mean Gaussian distributions can be straightforward by considering it as a Gaussian envelope problem with a nonzero mean (Sayim 2003). In the case of the TC model bias, defined as  $\bar{\mu}_{trop}$ , the true vertical protection level  $VPL_{true}$  is given by

$$VPL_{true} = k \sqrt{\sum_{n=1}^N S_z^2 \sigma_n^2 + \sum_{n=1}^N S_z \bar{\mu}_{trop}} \tag{12}$$

where  $N$  is the number of satellites.  $k$  is the multiplier which determines the probability of fault-free missed detection.  $S_z$  is the element of the third column of projection matrix.  $\sigma_n$  is the uncertainty of each ranging measurement.

The inflated vertical protection level is defined as  $VPL_{inflated}$

$$VPL_{inflated} \geq VPL_{true} \tag{13}$$

If equation (13) is true, the aircraft position error bound is expected and its integrity can be guaranteed. Equation (13) can be rewritten as,

$$k \sqrt{\sum_{n=1}^N S_z^2 \sigma_{inflated}^2} \geq \frac{k \sqrt{\sum_{n=1}^N S_z^2 \sigma_n^2 + \sum_{n=1}^N S_z \bar{\mu}_{trop}}}{k \sqrt{\sum_{n=1}^N S_z^2 \sigma_n^2}} k \sqrt{\sum_{n=1}^N S_z^2 \sigma_n^2} \tag{14}$$

where  $\sigma_{inflated}$  is the uncertainty that is inflated after taking into account the TC model bias. By employing the inflated model uncertainty, the requirement for overbounding is effectively satisfied with (Sayim 2003)

$$k \sqrt{\sum_{n=1}^N S_z^2 \sigma_{inflated}^2} \geq \xi k \sqrt{\sum_{n=1}^N S_z^2 \sigma_n^2} \tag{15}$$

where  $\xi$  is the inflation factor. According to equations (14) and (15), the inflation factor is given by

$$\xi = \left( 1 + \frac{\sum_{n=1}^N S_z \bar{\mu}_{trop}}{k \sqrt{\sum_{n=1}^N S_z^2 \sigma_n^2}} \right) \tag{16}$$

It can be found that the inflation factor is a function of the TC model bias and uncertainty of aircraft measurements. Although it is difficult to know the real measurement error of an aircraft, it is easy to determine the uncertainty of observations under conservative assumptions.

According to Fig. 16, there is a significant bias when the elevation is lower than around 20°. To reduce the risk of GBAS integrity, a variance inflation method with a threshold of 20° is used. In this method,  $\bar{\mu}_{trop}$  is 0 when the elevation

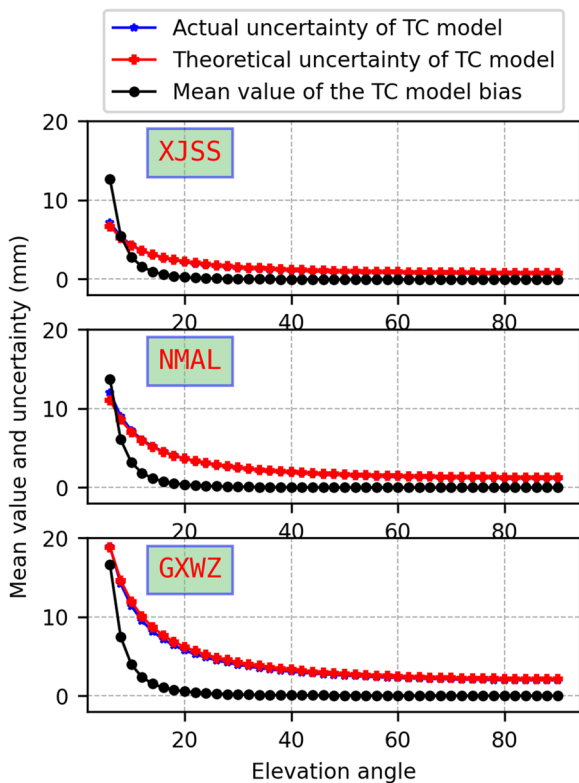


**Fig. 16** Variations of uncertainty and averaged bias of the TC model as a function of elevation angles at XJSS, NMAL and GXWZ stations in 2021. The cutoff elevation angle is 6°



exceeds  $20^\circ$ , which results in a value of 1 for  $\xi$ . In other words, the uncertainty of the TC model does not need to be inflated. When the elevation is lower than  $20^\circ$ ,  $\bar{\mu}_{\text{trop}}$  is shown by the black line in Fig. 16. Thus,  $\bar{\mu}_{\text{trop}}$  is given by

$$\bar{\mu}_{\text{trop}} = \begin{cases} B_{\text{Mean}} & \theta \leq 20^\circ \\ 0 & \theta > 20^\circ \end{cases} \quad (17)$$

where  $B_{\text{Mean}}$  is the TC model bias mean between the values calculated by the modified ray-tracing algorithm and the TC model in GBAS.

## Conclusions and remarks

The study investigated the performance of the existing TC models which use four different scale height estimation methods in GBAS. A modified ray-tracing algorithm is proposed to calculate the tropospheric delay error, thus providing a reference for evaluating the accuracy of TC models. The hourly ERA5 and CMONOC data in the whole year of 2021 in China were processed. Based on the analysis, the following conclusions can be drawn.

- 1) For the evaluation of the performance of the TC model in the zenith direction, the TC model bias calculated using the four scale height estimation methods shows approximate consistency in GAST-C. This answers which scale height estimation method should be used in TC model in China. Additionally, it can be concluded that as long as the input surface meteorological parameters are the same, a similar modeling accuracy can be attained by depicting the refractivity index profile as a straightforward linear profile. However, the TC model bias increases as the aircraft decision height rises. At a height of 400 m, the average bias of the TC model in the zenith direction reaches 1.34 mm, with an RMS of 10.38 mm. This is primarily attributed to the overall modeling approach of the TC model. Although the average bias is small, the maximum TC model bias reaches 28 mm. The presence of large TC model bias, which exceeds the range assured by the broadcasted tropospheric uncertainty, can cause loss of integrity. Therefore, carefully considering and bounding the TC model bias is essential to ensure flight safety.
- 2) In terms of the performance of the TC model in difference regions in China, the TC model bias from the 13 stations revealed notable variations, which is influenced by surface meteorological elements. The majority of stations exhibit a maximum bias in the zenith direction exceeding 10 mm with an anomaly occurrence probability exceeding 20% based on the worst-case

scenario. Among all the stations, GDZH presents the highest probability of experiencing a tropospheric anomaly, with a likelihood of 47%. This discrepancy can be attributed to the influence of low latitudes with more precipitation and higher temperatures, which leads to a higher probability of extreme weather events.

- 3) Regarding the MF-induced TC model bias in the slant direction, the TC model is almost unbiased when the elevation exceeds  $20^\circ$  at nominal conditions. However, a significant TC model bias arises for elevations below  $20^\circ$  due to the limitations of MF. Considering the fact that the magnitude of MF-induced bias is related to local climatic conditions and elevations, it is advisable not to applying a fixed inflation factor, as it may increase the TC model uncertainty and reduce the GBAS continuity. In extreme weather conditions, the TC model bias tends to increase as the elevation decreases. The maximum TC model bias found at an elevation of  $6^\circ$  is 363 mm. In terms of the TC model uncertainty, it is found that the distribution of the TC model bias deviates the Gaussian distribution. To reduce the influence of the MF and the non-Gaussian distribution of TC model bias on the integrity and continuity in GBAS, it is recommended to estimate the inflation factor dynamically based on real-time meteorological data. The strategy to define the dynamic inflation factor to overbound the GBAS MF-induced TC model bias will be the focus of the follow-on work. The development of a more precise MF will be also studied.

This study contributes to a better understanding of the GBAS TC model performance in China. In addition, it can provide valuable insights and guidance for developing more accurate TC models.

**Acknowledgements** The authors would like to thank the researchers and engineers at the National Key Laboratory of CNS/ATM for their advices and interests. The work was carried out with the financial support from the National Key Research and Development Program of China (grant nos. 2020YFB0505603), the National Natural Science Foundation of China (grant nos. 62022012, 62101019, U2033215 and U2233217), the Civil Aviation Security Capacity Building Fund Project (grant nos. CAAC Contract 2020(123), CAAC Contract 2021(77) and CAAC Contract 2022(110)).

**Author contributions** YZ and HT initiated the study. HT and KG wrote the manuscript with support from ZW. SW and YW helped to collect data and provided some helpful suggestions. All authors provided critical feedbacks and approved the manuscript.

**Data availability** ERA5 and meteorological datasets were obtained from <https://cds.climate.copernicus.eu/> and <https://data.earthquake.cn/>, respectively.

## Declarations

**Conflict of interest** The authors declare that they have no competing interests.

## References

- Askne J, Nordius H (1987) Estimation of tropospheric delay for microwaves from surface weather data. *Radio Sci* 22(3):379–386. <https://doi.org/10.1029/RS022i003p00379>
- Born M, Wolf E (1999) Principles of optics, 7th edn. Cambridge University Press, New York
- Chao CC (1974) The tropospheric calibration model for Mariner Mars 1971. NASA Technical Report 32-1587. National Aeronautics and Space Administration. <https://ntrs.nasa.gov/api/citations/1974008866/downloads/1974008866.pdf>. Accessed 6 June 2023
- Davis JL, Herring TA, Shapiro II, Rogers AEE, Elgered G (1985) Geodesy by radio interferometry: effects of atmospheric modeling errors on estimates of baseline length. *Radio Sci* 20(6):1593–1607. <https://doi.org/10.1029/RS020i006p01593>
- Haji Aghajany S, Amerian Y (2017) Three dimensional ray tracing technique for tropospheric water vapor tomography using GPS measurements. *J Atmos Solar Terr Phys* 164:81–88. <https://doi.org/10.1016/j.jastp.2017.08.003>
- Hobiger T, Ichikawa R, Koyama Y, Kondo T (2008) Fast and accurate ray-tracing algorithms for real-time space geodetic applications using numerical weather models. *J Geophys Res* 113:D20302. <https://doi.org/10.1029/2008JD010503>
- Hobiger T, Kinoshita Y, Shimizu S, Ichikawa R, Furuya M, Kondo T, Koyama Y (2010) On the importance of accurately ray-traced troposphere corrections for interferometric SAR data. *J Geod* 84(9):537–546. <https://doi.org/10.1007/s00190-010-0393-3>
- Hofmeister A, Böhm J (2017) Application of ray-traced tropospheric slant delays to geodetic VLBI analysis. *J Geod* 91(8):945–964. <https://doi.org/10.1007/s00190-017-1000-7>
- Hopfield HS (1971) Tropospheric effect on electromagnetically measured range: prediction from surface weather data. *Radio Sci* 6(3):357–367. <https://doi.org/10.1029/RS006i003p00357>
- Khanafseh S, Von Engeln A, Pervan B (2016) Tropospheric duct anomaly threat model for high integrity and high accuracy navigation. In: Proceedings ION GNSS+ 2016, Institute of Navigation, Portland, Oregon, USA, September 12–16, pp 1609–1616. <https://doi.org/10.33012/2016.14662>
- Leandro R, Santos M, Langley RB (2006) UNB neutral atmosphere models: development and performance. In: Proceedings ION NTM 2006, Institute of Navigation, Monterey, CA, USA, January 18–20, pp 564–573
- McCarthy DD, Petit G (2004) IERS conventions 2003. IERS technical note 32, Verlag des Bundesamts für Kartographie und Geodäsie, Frankfurt am Main
- McGraw GA, Murphy T, Brenner M, Pullen S, Van Dierendonck AJ (2000) Development of the LAAS accuracy models. In: Proceedings ION GPS 2000, Institute of Navigation, Salt Lake City, UT, USA, September 19–22, pp 1212–1223
- McGraw GA (2012) Tropospheric error modeling for high integrity airborne GNSS navigation. In: Proceedings IEEE/ION PLANS 2012, Institute of Navigation, Myrtle Beach, South Carolina, USA, April 24–26, pp 158–166
- Nafisi V, Urquhart L, Santos MC, Nievinski FG, Bohm J, Wijaya DD, Schuh H, Ardalan AA, Hobiger T, Ichikawa R, Zus F, Wickert J, Gegout P (2012) Comparison of ray-tracing packages for troposphere delays. *IEEE Trans Geosci Remote Sens* 50(2):469–481. <https://doi.org/10.1109/TGRS.2011.2160952>
- Peng S (2020) 1-km monthly precipitation dataset for China (1901–2022). Big Earth Data Platform Three Poles. <https://doi.org/10.5281/zenodo.3185722>
- RTCA (2004) Minimum aviation system performance standards for the local area augmentation system (LAAS). Tech Rep DO-245A, RTCA, Washington DC
- RTCA (2017) Minimum operational performance standards for GPS local area augmentation system airborne equipment. Tech Rep DO-253D, RTCA, Washington DC
- Saito S, Sunda S, Lee J, Pullen S, Supriadi S, Yoshihara T, Terkildsen M, Lecat F (2017) Ionospheric delay gradient model for GBAS in the Asia-Pacific region. *GPS Solut* 21(4):1937–1947. <https://doi.org/10.1007/s10291-017-0662-1>
- Saito S, Yoshihara T, McGraw G, Harris M (2021) Agenda Item 3: SARPs for GNSS elements and signals (GBAS), guidance on the tropospheric scale height. JWG/7-WP/6, international civil aviation organization navigation systems panel
- Saito S, Yoshihara T, McGraw G, Martinez G, Lavik L, Topland M (2022) Agenda Item 3: SARPs for GNSS elements and signals (GBAS), validation and proposals of the guidance on the tropospheric parameters for GBAS. JWG/9-WP/25, international civil aviation organization navigation systems panel
- Sayim I (2003) Ranging error overbounds for navigation integrity of local area augmented GPS. Dissertation, Illinois Institute of Technology
- Sheng PX, Mao JT, Li JG, Ge ZM, Zhang AC, Sang JG, Pan NX, Zhang HS (2013) Atmosphere physics, 2nd edn. Peking University Press, Beijing
- Shi H, Zhang R, Nie Z, Li Y, Chen Z, Wang T (2018) Research on variety characteristics of mainland China troposphere based on CMONOC. *Geodesy Geodyn* 9(5):411–417. <https://doi.org/10.1016/j.geog.2018.06.00>
- Skidmore TA, van Graas F (2004) An investigation of tropospheric errors on differential GNSS accuracy and integrity. In: Proceedings ION GNSS 2004, Institute of Navigation, Long Beach, CA, USA, September 21–24, pp 2752–2760
- Song Y, Achberger C, Linderholm HW (2011) Rain-season trends in precipitation and their effect in different climate regions of China during 1961–2008. *Environ Res Lett* 6(3):034025. <https://doi.org/10.1088/1748-9326/6/3/034025>
- Thayer GD (1967) A Rapid and Accurate Ray Tracing Algorithm for a Horizontally Stratified Atmosphere. *Radio Sci* 2(2):249–252. <https://doi.org/10.1002/rds196722249>
- Thayer GD (1974) An improved equation for the radio refractive index of air. *Radio Sci* 9(10):803–807. <https://doi.org/10.1029/RS009i010p00803>
- Wallace JM, Hobbs PV (2006) Atmospheric thermodynamics. Atmospheric science: an introductory survey, vol 3, 2nd edn. Academic Press, pp 63–111
- Wang J, Balidakis K, Zus F, Chang X, Ge M, Heinkelmann R, Schuh H (2022) Improving the vertical modeling of tropospheric delay. *Geophys Res Lett* 49(5):e2021GL096732. <https://doi.org/10.1029/2021GL096732>
- Warburton J (2010) Tropospheric error bounding: nominal and anomalous tropospheric conditions parameter calculation and consistency. Federal Aviation Administration. <https://laas.tc.faa.gov/documents/CAAC/CAAC%2011%20Tropospheric%20Threat.pdf>. Accessed 6 June 2023
- Zhang M, Zhang K, Wu S, Shi J, Li L, Wu H, Liu S (2022) A new method for tropospheric tomography using GNSS and Fengyun-4A data. *Atmos Res* 280:106460. <https://doi.org/10.1016/j.atmosres.2022.106460>
- Zhou Y, Lou Y, Zhang W, Kuang C, Liu W, Bai J (2020) Improved performance of ERA5 in global tropospheric delay retrieval. *J Geod* 94(10):103. <https://doi.org/10.1007/s00190-020-01422-3>

**Publisher's Note** Springer Nature remains neutral with regard to jurisdictional claims in published maps and institutional affiliations.

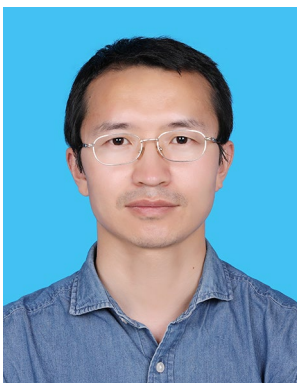
Springer Nature or its licensor (e.g. a society or other partner) holds exclusive rights to this article under a publishing agreement with the author(s) or other rightsholder(s); author self-archiving of the accepted manuscript version of this article is solely governed by the terms of such publishing agreement and applicable law.



**Yanbo Zhu** received his B.S. degree and Ph.D. degree from Beihang University in 1995 and 2009. He is a professor at the National Key Lab of CNS/ATM and the chief engineer at Aviation Data Communication Corporation. His research interests are satellite navigation, datalink communication and automatic dependent surveillance.



**Honglin Tang** received B.S. and M.Sc. degrees in Shandong Jianzhu University in 2017 and Chang'an University in 2020. He currently is a doctoral candidate in the National Key Laboratory of CNS/ATM at Beihang University. His research interests concentrate on tropospheric anomaly monitoring for GBAS.



**Zhipeng Wang** received his B.S. in Communication Engineering from Northwestern Polytechnical University (NWPU) in 2006 and his Ph.D. in Traffic Information Engineering from Beihang University in 2013. He is a professor at the Department of Electronic Information Engineering, Beihang University, China. His research focuses on high precision aviation navigation Minimum Operation Network (MON), aviation navigation integrity monitoring, GNSS aviation application test verification and international standardization.



**Kai Guo** is an Associate Professor at the Institute of Artificial Intelligence at Beihang University. He received his Ph.D. in Engineering Surveying and Space Geodesy from the Nottingham Geospatial Institute, University of Nottingham in 2021. He was a Marie Skłodowska-Curie research fellow since 2017. His research has focused on ionospheric effects on GNSS and aviation navigation.



**Shujing Wang** received the M.S. degree in Electronic and Communication Engineering from School of Electronic and Information Engineering, Beihang University in 2018. He is currently a Ph.D. candidate in School of Electronic and Information Engineering, Beihang University of CNS/ATM laboratories. His major research interests are GBAS, aviation navigation and aeronautical telecommunication network.



**Yiming Wang** received his B.S. and M.Sc. degrees in Civil Aviation University of China (CAUC) in 2019 and 2022. He is currently working toward a Ph.D. degree in the School of Electronics and Information Engineering, Beihang University. His research interests concentrate on the interference and jamming mitigation algorithms of GNSS.